Synthesis and Characterization of Diiron(III)-Substituted Silicotungstate, $[\gamma(1,2)\text{-}SiW_{10}\{Fe(OH_2)\}_2O_{38}]^{6-}$

Chika Nozaki,[†] Ikuro Kiyoto,[†] Yoshitaka Minai,[‡] Makoto Misono,[†] and Noritaka Mizuno*,[†]

Department of Applied Chemistry, Graduate School of Engineering, The University of Tokyo, Hongo, Bunkyo-ku, Tokyo 113-8656, Japan, and Center for Arts and Science, Faculty of Humanities, Musashi University, Toyotama-kami, Nerima-ku, Tokyo 176-0011, Japan

Received February 22, 1999

The full details of synthesis and characterization of diiron(III)-substituted γ-Keggin silicotungstate, $[\gamma(1,2)\text{-}SiW_{10}\{Fe(OH_2)\}_2O_{38}]^{6-}$ (abbreviated as **I**) were reported. This complex was synthesized by the reaction of the lacunary $[\gamma\text{-}SiW_{10}O_{36}]^{8-}$ with $Fe(NO_3)_3$ in an acidic aqueous solution and isolated as the tetra-*n*-butylammonium salt (TBA-**I**). TBA-**I** has been characterized by infrared, Raman, ^{183}W NMR, UV−visible, Mössbauer, and ESR spectroscopy, TG/DTA, FAB-mass, and magnetic susceptibility measurements, elemental analysis, and acid/base titration. The ^{183}W NMR, infrared, Raman, and UV−visible spectroscopy indicated that **I** has a γ-Keggin structure with C_{2v} symmetry. It was shown by the magnetic susceptibility measurement and Mössbauer, ESR, and UV−visible spectroscopy that **I** shows an antiferromagnetic coupling of the two high-spin Fe^{3+} centers.

Introduction

Catalytic function of polyoxometalates has attracted much attention because their acidic and redox properties can be controlled at atomic or molecular levels.[1−8] The strong acidity or oxidizing property of polyoxometalates induces a lot of studies on the heterogeneous and homogeneous catalysis. The additional attractive and technologically significant aspects of polyoxometalates in catalysis are their inherent stability toward oxygen donors such as molecular oxygen and hydrogen peroxide. For example, high stability toward hydrogen peroxide has been reported for manganese- or iron-substituted polyoxometalates.[9−15] Therefore, polyoxometalates are useful catalysts for liquid-phase oxidations of various organic substrates with hydrogen peroxide.

Iron is known to exhibit significant catalytic activity in biological and synthetic systems.[16,17] Diiron-containing hemerythrin, ribonucleotide reductase, and methane monooxygenase are the prominent examples of the redox-active enzymes. The active site of methane monooxygenase has already been shown to have a μ-hydroxo diiron structure.[18]

There are several examples of iron-containing polyoxometalates, mono and triiron-substituted Keggin-type silicotungstates,[13,14] Fe_2Ni-substituted Keggin-type phosphotungstate,[15] and tetrairon-containing Dawson- and Keggin-derived sandwich compounds.[10,11] However, diiron-substituted silicotungstate, $[\gamma\text{-}SiW_{10}\{Fe(OH_2)\}_2O_{38}]^{6-}$ (**I**), has never been reported.

Recently, we have reported (1) that the tetra-*n*-butylammonium salt of diiron-substituted silicotungstate (TBA-**I**) can catalyze selective oxidation of alkanes and alkenes with highly efficient utilization of hydrogen peroxide,[19,20] including the preliminary characterization,[19] (2) that even methane is catalytically oxidized by **I** with hydrogen peroxide,[21] and (3) that structures of iron centers remarkably influence the catalytic activities, TBA-**I** being specifically the most active among non-, mono-, di-, and triiron–substituted silicotungstates.[21a] Therefore, the investigation of the structure of **I** in more detail is important for understanding the oxidation catalysis. In this paper, we report the full details of synthesis, isolation, and characterization of TBA-**I** (Figure 1).

[†] The University of Tokyo.
[‡] Musashi University.

(1) Kozhevnikov, I. V. *Chem. Rev.* **1998**, *98*, 171−198.
(2) Neumann, R. *Prog. Inorg. Chem.* **1998**, *47*, 317−370.
(3) Mizuno, N.; Misono, M. *Chem. Rev.* **1998**, *98*, 199−217.
(4) Okahara, T.; Mizuno, N.; Misono, M. *Adv. Catal.* **1996**, *41*, 113−252.
(5) Hill, C. L.; Prosser-McCartha, C. M. *Coord. Chem. Rev.* **1995**, *143*, 407−453.
(6) Pope, M. T.; Müller, A. *Angew. Chem., Int. Ed. Engl.* **1991**, *30*, 34−48.
(7) Hill, C. L. *Activation and Functionalization of Alkanes*; Wiley: New York, 1989; p 243−279.
(8) Pope, M. T. *Heteropoly and Isopoly Oxometalates*; Springer-Verlag: Berlin, 1983.
(9) Bösing, M.; Nöh, A.; Loose, I.; Krebs, B. *J. Am. Chem. Soc.* **1998**, *120*, 7252−7259.
(10) Zhang, X.; Chen, Q.; Duncan, D. C.; Campana, C. F.; Hill, C. L. *Inorg. Chem.* **1997**, *36*, 4208−4215.
(11) Zhang, X.; Chen, Q.; Duncan, D. C.; Lachicotte, R. J.; Hill, C. L. *Inorg. Chem.* **1997**, *36*, 4381−4386.
(12) Neumann, R.; Gara, M. *J. Am. Chem. Soc.* **1994**, *116*, 5509−5510.
(13) Zonnevijille, F.; Tourné, C. M.; Tourné, G. F. *Inorg. Chem.* **1982**, *21*, 2751−2757.
(14) Liu, J.; Ortéga, F.; Sethuraman, P.; Katsoulis, D. E.; Costello, C. E.; Pope, M. T. *J. Chem. Soc., Dalton Trans.* **1992**, 1901−1906.
(15) Mizuno, N.; Hirose, T.; Tateishi, M.; Iwamoto, M. *J. Mol. Catal.* **1994**, *88*, L125−L131.
(16) Powell, A. K. *Struct. Bonding* **1992**, *88*, 1−225.
(17) Holm, R. H.; Kennepohl, P.; Solomon, E. I. *Chem. Rev.* **1996**, *96*, 2239−2314.
(18) Rosenzweig, A. C.; Frederick, C. A.; Lippard, S. J.; Nordland, P. *Nature* **1993**, *366*, 537−543.
(19) Mizuno, N.; Nozaki, C.; Kiyoto, I.; Misono, M. *J. Am. Chem. Soc.* **1998**, *120*, 9267−9272.
(20) Mizono, N.; Nozaki, C.; Kiyoto, I.; Misono, M. *J. Catal.* **1999**, *182*, 285−288.
(21) (a) Mizuno, N.; Kiyoto, I.; Nozaki, C.; Misono, M. *J. Catal.* **1999**, *181*, 171−174. (b) Mizuno, N.; Seki, Y.; Nishiyama, Y.; Kiyoto, I.; Misono, M. *J. Catal.* **1999**, *184*, 550−552.

10.1021/ic9902065 CCC: $18.00
Published on Web 11/12/1999

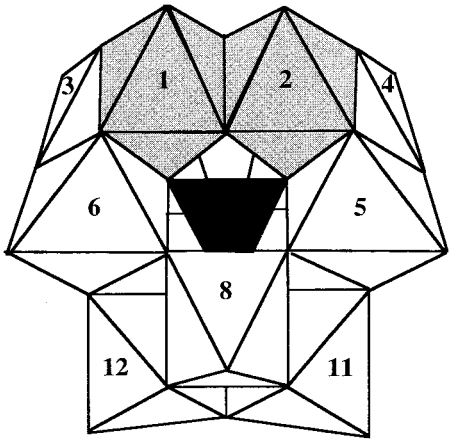

Figure 1. Polyhedral representation of diiron-substituted Keggin-type silicotungstate (**I**). The two iron atoms are represented by shaded octahedra. WO_6's occupy the white octahedra, and an SiO_4 group is shown as the internal black tetrahedron. The W*n* represents the number of the WO_6 site in the Keggin structure. The numbering is based on IUPAC recommendations.[60]

Experimental Section

Materials. $Fe(NO_3)_3 \cdot 9H_2O$ (Koso Chemical Co., Ltd.), acetonitrile (Nacalai Tesque, Inc.), acetonitrile-d_3 (Isotec, Inc.), and tetra-*n*-butylammonium nitrate (Aldrich) were commercially obtained and used as received. Tetra-*n*-butylammonium hydroxide (abbreviated as TBA(OH)) was prepared according to ref 22. $K_8[\gamma\text{-}SiW_{10}O_{36}] \cdot 12H_2O$ was prepared according to ref 23, and its purity was confirmed by the infrared spectrum. $[(n\text{-}C_4H_9)_4N]_4[\gamma(1,2)\text{-}SiW_{10}Mn^{III,III}{}_2O_{40}H_6] \cdot 1.5CH_3CN \cdot 2H_2O$ was prepared according to ref 24, and the structure was characterized by infrared, UV−visible, and ESR spectroscopy.

Instrumentation/Analytical Procedures. Elemental analysis was performed by Mikroanalytisches Labor Pascher (Remagen, Germany). Spectroscopic measurements were carried out at room temperature unless otherwise stated. Infrared spectra in the range of 400−4000 cm^{-1} (KBr disks) were measured with a JASCO FT/IR-550 spectrometer. Infrared spectra below 600 cm^{-1} (CsI disks) were measured with a JASCO FT-IR/620 spectrometer. Raman spectra were recorded on a T-64000 (JOBIN YVON) spectrometer using a GLS 3450J argon laser (488 nm, ∼100 mW). Thermogravimetric analyses (TGA) were carried out in N_2 with a SSC/5200 thermal gravimetric analyzer (Seiko Instruments). UV−visible spectra were recorded on a Lambda 12 UV/vis spectrometer (Perkin Elmer). Magnetic susceptibility data were recorded on a SQUID susceptometer (Quantum Design MPMSXL). Mössbauer spectra were recorded in a similar way to that described in ref 15. ESR measurements were made at X-band using a Bruker ESP 300E spectrometer. Fast atom bombardment (FAB) mass spectra were recorded on CONCEPT 1H (SHIMADZU/KRATOS). ^{183}W NMR (11.2 MHz) spectra were recorded in 10 mm o.d. tubes on a JEOL JMN-EX-270 FT-NMR spectrometer. The saturated $Na_2WO_4-D_2O$ solution was used as an external reference. Chemical shifts were reported on the δ scale with resonance upfield of Na_2WO_4 ($\delta = 0$) as negative.

Synthesis of $[(n\text{-}C_4H_9)_4N]_{3.5}H_{2.5}[\gamma\text{-}SiW_{10}\{Fe(OH_2)\}_2O_{38}] \cdot H_2O$ (TBA-I). The present preparation was carried out by a major modification of the method reported for the synthesis of $[(n\text{-}C_4H_9)_4N]_4[\gamma(1,2)\text{-}(SiO_4)W_{10}Mn^{III,III}{}_2O_{36}H_6] \cdot 1.5CH_3CN \cdot 2H_2O$.[24] A solution of $K_8[\gamma\text{-}SiW_{10}O_{36}] \cdot 12H_2O$ (3.0 g, 1.0 mmol) in 30 mL of deionized water was quickly adjusted to pH = 3.90 with concentrated nitric acid. Then, an aqueous solution ($Fe(NO_3)_3 \cdot 9H_2O$ (0.82 g, 2.0 mmol) in 5 mL of water) was added. The color of the solution turned to pale yellow. After the solution had been stirred for 5 min, the addition of an excess amount of tetra-*n*-butylammonium nitrate (3.1 g, 10 mmol) resulted in a white-yellow precipitate. The precipitate was filtered off and purified by twice dissolving it in acetonitrile (15 mL) and then water (300 mL) to reprecipitate the product. The yield of the purified compound was about 1.5 g (50 %). The yellow-orange powder was soluble in acetonitrile and dichloroethane, and slightly soluble in dichloromethane, but insoluble in water. UV−visible in CH_3CN (λ_{max}, nm (ϵ, M^{-1} cm^{-1})): 275 (22 600), 334 (10 000), 470 (68). Elemental Anal. Found (calcd) for $[(n\text{-}C_4H_9)_4N]_{3.5}H_{2.5}[\gamma\text{-}SiW_{10}\{Fe(OH_2)\}_2O_{38}] \cdot H_2O$: C, 19.48 (19.26); H, 3.71 (3.88); N, 1.47 (1.40); Si, 0.85 (0.80); Fe, 2.64 (3.20); W 54.0 (52.7) (6 elements) (the data were fairly complete). The contents of Si and Fe for our ICP analyses were 0.80 and 3.20, respectively. TGA: Weight loss between 300 and 445 K was 1.9 % (calcd for $3H_2O$ in TBA-**I**, 1.5%).

Acid/Base Titration of TBA-I. The titration was carried out with TBA(OH) according to ref 25. TBA-**I** (0.020 g) was dissolved in a solvent mixture of 15 mL/400 μL acetonitrile/water (400 μL). The solution was placed in dry Ar and stirred at room temperature. The titration data were obtained with a HM-30 pH meter (TOA Electrochemical Measuring Instruments). Data points were obtained in millivolts. The potential was monitored as a solution of TBA(OH) (0.1 M) was syringed into the solution in 0.2 equiv intervals.

Results and Discussion

Synthesis. Stoichiometric amounts of $K_8[\gamma\text{-}SiW_{10}O_{36}] \cdot 12H_2O$ (1.0 mmol) and $Fe(NO_3)_3 \cdot 9H_2O$ (2.0 mmol) were mixed at pH = 3.9 and room temperature (eq 1) and **I** was isolated as the hydrophobic quaternary tetrabutylammonium salt. Key points in the synthesis of TBA-**I** were removal of an excess of $[(n\text{-}C_4H_9)_4N]NO_3$ and the reaction temperature. The purification (i.e., removal of excess $TBA(NO_3)$ was accomplished by dissolving the white-yellow solid and then adding water to precipitate yellow-orange powder. The yellow-orange precipitate, TBA-**I**, was obtained in 50% yield.[26] When the synthetic solution was heated at 353−363 K for 2 h, a new weak UV−visible band appeared at 278 nm, characteristic of the β-Keggin structure.[27] This fact shows the isomerization. The isomerization at elevated temperatures has been reported for $[\gamma\text{-}SiW_{12}O_{40}]^{4-}$,[27] supporting the idea.

$$[\gamma(1,2)\text{-}SiW_{10}O_{36}]^{8-} + 2Fe(NO_3)_3 \xrightarrow[\text{excess } TBANO_3]{pH = 3.9} [\gamma(1,2)\text{-}SiW_{10}\{Fe(OH_2)\}_2O_{38}]^{6-} \quad (1)$$

The molecular formula of TBA-**I** was established by the elemental analysis. The thermogravimetric analysis shows the presence of three H_2O in accordance with the data of elemental analyses. The molecular weight of the monomeric polyoxometalate, $SiW_{10}Fe_2O_{38}{}^{6-}$, is 2586.26, and that of the dimeric anion, for example, $[(SiW_{10}Fe_2O_{38})_2O_2]^{16-}$, is 5204.51. The negative ion FAB mass spectrum showed no intense peaks in the range of 4200−10000, in agreement with the monomer formulation of $SiW_{10}Fe_2O_{38}{}^{6-}$. The monomer formation is consistent with the usage of an aprotic solvent, acetonitrile, where the formation constant of dimer species is low, while Tourné et al. reported that iron(III)-containing silicotungstates are dimerized in an aqueous solution.[13]

Acid/Base Titration and Deprotonation of TBA-I. Figure 2 shows the titration curve of TBA-**I**. Two break points were observed at 2.5 and 4.5 equiv of added base. The deprotonation

(22) Cundiff, R. H.; Markunas, P. C. *Anal. Chem.* **1958**, *30*, 1450−1452.
(23) Tézé, A.; Hervé, G. *Inorg. Synth.* **1990**, *27*, 85−96.
(24) Zhang, X.; O'Connor, C. J.; Jameson, G. B.; Pope, M. T. *Inorg. Chem.* **1996**, *35*, 30−34.
(25) Edlund, D. J.; Saxton, R. J.; Lyon, D. K.; Finke, R. G. *Organometallics* **1988**, *7*, 1692−1704.
(26) Our attempts to grow crystallographic quality single crystals were carried out in organic solvents such as acetonitirile, 1,2-dichloroethane, dichloromethane, etc., using $[(n\text{-}C_4H_9)_4N]^+$, $(CN_3H_6)^+$, and $[(CH_3)_3(C_6H_5)N]^+$ as counter cations. To date, the crystallization has been unsuccessful and other attempts are in progress.
(27) Tézé, A.; Canny, J.; Gurban, L.; Thouvenot, R.; Hervé, G. *Inorg. Chem.* **1996**, *35*, 1001−1005.

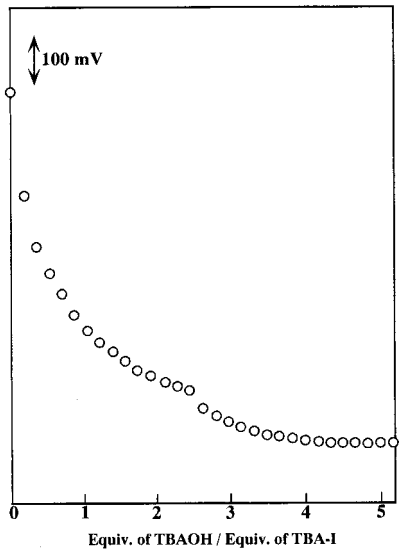

Figure 2. Millivolt titration of TBA-**I** with TBA(OH).

of water molecules bound to Fe^{3+} has been reported for $Fe_2O(phen)_4(OH_2)_2(NO_3)_4$[28] and $K_7[P_2W_{17}Fe(OH_2)O_{61}]$.[29] Protons of ligand water molecules are acidic and can be distinguished from free protons by the acid/base titration; e.g., $H_7As_2Fe(OH_2)W_{17}O_{61}$ has seven free protons and one titratable ligand proton and therefore two break points exist at ca. 7 and 8 equiv of added base.[13] Therefore, the observation of two break points for TBA-**I** shows that this compound has 2.5 free protons and 2 titratable ligand protons (i.e., 2 aquo ligands). The fact that the deprotonation of water molecules bound to Fe in $Fe_2O(phen)_4(OH_2)_2(NO_3)_4$ proceeds at pH 3−4,[28] where **I** was prepared, is consistent with the idea. The following two facts support the idea: (1) The infrared spectrum of TBA-**I** showed a broad band ($\nu_{1/2}$ = ca. 410 cm^{-1}) around 3450 cm^{-1} and no sharp ($\nu_{1/2}$ < 50 cm^{-1}) bands are observed above 3620 cm^{-1}, where isolated OH groups bound to Fe have bands.[30] (2) It has also been reported that water molecules bound to Fe give broad bands ($\nu_{1/2}$ = ca. 430 cm^{-1}) around 3400 cm^{-1},[31] and that bridging OH groups between metal ions of Fe, Cu, and Co give broad bands from 3300 to 3600 cm^{-1},[32−34] as observed for TBA-**I**.

It has been reported that $[(n\text{-}C_4H_9)_4N]_4[\gamma(1,2)\text{-}SiW_{10}Mn^{III,III}{}_2O_{40}H_6]\cdot 1.5CH_3CN\cdot 2H_2O$ has two free protons on bridging oxygens between manganese centers.[24] We synthesized the same sample, and a break point was observed at 2.0 equiv of added base. The observation is consistent with the report.

^{183}W NMR Spectrum. Tézé et al. characterized $[\gamma\text{-}SiW_{12}O_{40}]^{4-}$ and $[\gamma(1,2)\text{-}SiW_{10}V_2O_{40}]^{6-}$ with ^{183}W NMR spectroscopy.[27,35] Figure 3 shows the ^{183}W NMR spectrum of TBA-**I** in acetonitrile-d_3. The spectrum showed two peaks at −1334 and −1847 ppm with integrated intensities of 2:1, respectively.

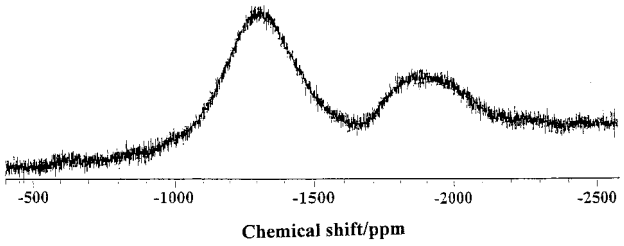

Figure 3. ^{183}W NMR spectrum of TBA-**I** in acetonitrile-d_3 at 296 K.

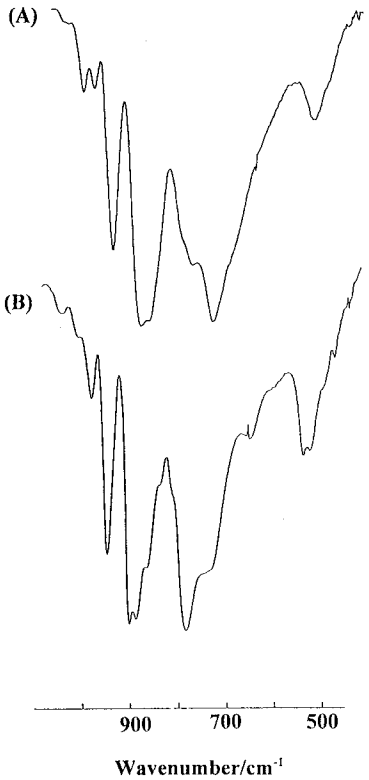

Figure 4. Infrared spectra of (A) TBA-**I** and (B) $[(n\text{-}C_4H_9)_4N]_4[\gamma(1,2)\text{-}SiW_{10}Mn^{III,III}{}_2O_{40}H_6]\cdot 1.5CH_3CN\cdot 2H_2O$ in the range of 400−1100 cm^{-1} (KBr disks).

According to the assignments of W*n* in $[\gamma(1,2)\text{-}SiW_{10}V_2O_{40}]^{6-}$,[35] the lower-field signal at −1334 ppm is assigned to equivalent W9−W10−W11−W12 atoms. The other signal at −1847 ppm is assigned to the W7 and W8 atoms. The signals due to W3−W4−W5−W6 atoms bound to FeO_5 were not observed because of the coupling with paramagnetic high-spin d^5 Fe^{3+}. A similar disappearance of ^{31}P and ^{183}W signals is observed for $\alpha_2\text{-}P_2W_{17}O_{61}(M^{n+}\cdot Br)^{(n-11)}$ (M = Mn^{3+}, Fe^{3+}, Co^{2+}, Ni^{2+}, Cu^{2+}) polyoxometalates.[36] The spectral pattern of TBA-**I** is analogous to that of $[\gamma(1,2)\text{-}SiW_{10}Mn^{II,II}{}_2O_{40}]^{12-}$, which was separately prepared according to the literature,[24] and two broad ^{183}W signals were observed at −1181 and −1700 ppm with 2:1 intensities, respectively. These facts clearly indicate that the two iron atoms occupy edge-shared octahedra at 1 and 2 positions.

Infrared and Raman Spectra. Infrared spectra of polyoxometaletes with various structures show characteristic bands in the region of 400−1200 cm^{-1}.[8] Parts A and B of Figure 4 show infrared spectra of (A) TBA-**I** and (B) $[(n\text{-}C_4H_9)_4N]_4[\gamma(1,2)\text{-}(SiO_4)W_{10}Mn^{III,III}{}_2O_{36}H_6]\cdot 1.5CH_3CN\cdot 2H_2O$, respectively. Figure 4A shows intense bands at 960, 902, 884, and 800 cm^{-1} with a very broad band at 753 cm^{-1}, and the spectral pattern is

(28) Duboc-Toia, C.; Ménage, S.; Vincent, J.; Averbuch-Pouchot, M. T.; Fontecave, M. *Inorg. Chem.* **1997**, *36*, 6148−6149.
(29) Contant, R.; Abbessi, M.; Jacqueline, C.; Belhouari, A.; Keita, B.; Nadjo, L. *Inorg. Chem.* **1997**, *36*, 4961−4967.
(30) Ishikawa, T.; Nitta, S.; Kondo, S. *J. Chem. Soc., Faraday Trans. 1* **1986**, *82*, 2401−2410.
(31) Nyquist, R. A.; Kagel, R. O. *Infrared Spectra of Inorganic Compounds;* Academic Press: New York and London, 1971.
(32) Ferraro, J. R.; Driver, R.; Walker, W. R.; Wozniak, W. *Inorg. Chem.* **1967**, *6*, 1586−1588.
(33) Ferraro, J. R.; Basile, L. J.; Kovacic, D. L. *Inorg. Chem.* **1966**, *5*, 391−395.
(34) Ferraro, J. R.; Walker, W. R. *Inorg. Chem.* **1965**, *4*, 1382−1386.
(35) Canny, J.; Thovenot, R.; Tézé, A.; Hervé, G.; Leparulo-Loftus, M.; Pope, M. T. *Inorg. Chem.* **1991**, *30*, 976−981.
(36) Lyon, D. K.; Miller, W. K.; Novet, T.; Domaille, P. J.; Evitt, E.; Johnson, D. C.; Finke, R. G. *J. Am. Chem. Soc.* **1991**, *113*, 7209−7221.

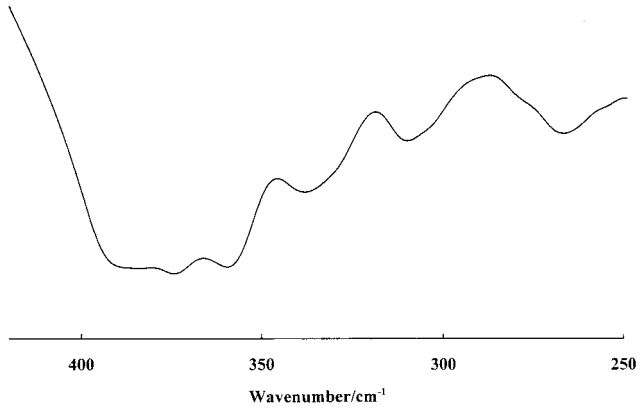

Figure 5. Infrared spectrum of TBA-**I** below 600 cm^{-1} (CsI disk).

analogous to Figure 4B (958 (s), 911 (s), 897 (s), and 792 (s, br) cm^{-1}). In the range of 250−1000 cm^{-1}, the Raman spectrum of TBA-**I** showed bands at 974, 955, and 220 cm^{-1}, characteristic of the Keggin structure.[37]

It has been reported that the low-frequency regions (below 420 and 250 cm^{-1} for infrared and Raman spectra, respectively) can be used to distinguish α- and β-Keggin silicotungstates from the γ-isomer.[27] Figure 5 shows the infrared spectrum of TBA-**I** in the range of 250−420 cm^{-1}. Six bands were observed with very similar intensity ratios to those of $[\gamma\text{-}SiW_{12}O_{40}]^{4-}$. It has been reported that the number of infrared bands increases from 3 to 6 with a decrease in the symmetry from α- to γ-Keggin silicotungstate.[27] Therefore, the agreement of the band number of TBA-**I** with that of $[\gamma\text{-}SiW_{12}O_{40}]^{4-}$ suggests that TBA-**I** has a γ-Keggin structure. In addition, the lowest-frequency of IR bands for α-, β-, and γ-Keggin silicotungstates appear at 288, 280, and 277 cm^{-1}, respectively, and decrease with the decrease in the symmetry.[27] The lowest-frequency of band for TBA-**I** was 267 cm^{-1} and lower than those for α- and β-Keggin silicotungstates in accord with the γ-Keggin structure of TBA-**I**.

It has also been reported that the lowest-frequency of Raman bands for α-, β-, and γ-Keggin silicotungstates appear at 90, 73, and 64 cm^{-1}, respectively. The band position for TBA-**I** was 59 cm^{-1}. The value is lower than those for α- and β-Keggin silicotungstates and in close agreement with that of the $[\gamma\text{-}SiW_{12}O_{40}]^{4-}$, also supporting the γ-Keggin structure of TBA-**I**.

UV−Visible Spectrum. It has been reported that the number of UV bands increases with a decrease in the symmetry of Keggin-type polyoxometalates:[27,38] The UV−visible spectrum of α-dodecatungstosilicate shows one narrow line (λ_{max} = 262 nm, $\epsilon = 4.2 \times 10^4$ M^{-1} cm^{-1}). The band splits into two broad bands (λ_{max} = 264 nm, $\epsilon = 3 \times 10^4$ M^{-1} cm^{-1}; λ_{max} = 236 nm, $\epsilon = 2.7 \times 10^4$ M^{-1} cm^{-1}) for the β-isomer. The UV−visible spectrum of TBA-**I** is shown in Figure 6. Similarly to $[\gamma\text{-}SiW_{12}O_{40}]^{4-}$,[27] two broader shoulders were observed at 275 nm (ϵ = 22 600 M^{-1} cm^{-1}) and 334 nm (ϵ = 10 000 M^{-1} cm^{-1}).

As shown in an inset of Figure 6, an additional shoulder band was observed at 470 nm (ϵ = 68 M^{-1} cm^{-1}). The band is assigned to the $O \rightarrow Fe^{3+}$ charge transfer band according to

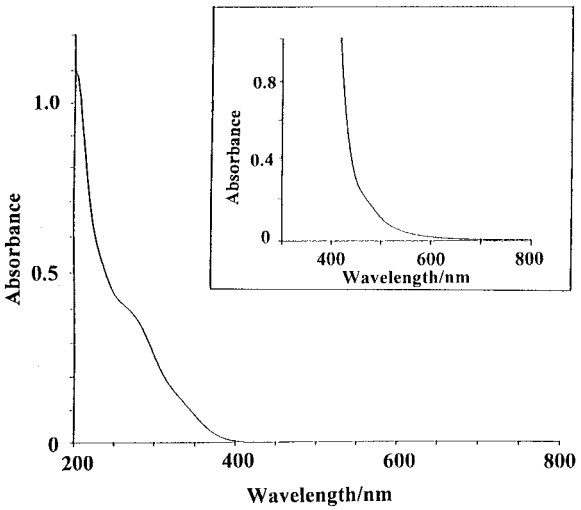

Figure 6. UV−visible spectrum of TBA-**I** in acetonitrile (1.6×10^{-5} M). Inset: Absorption spectrum of TBA-**I** in acetonitrile (2.8×10^{-3} M).

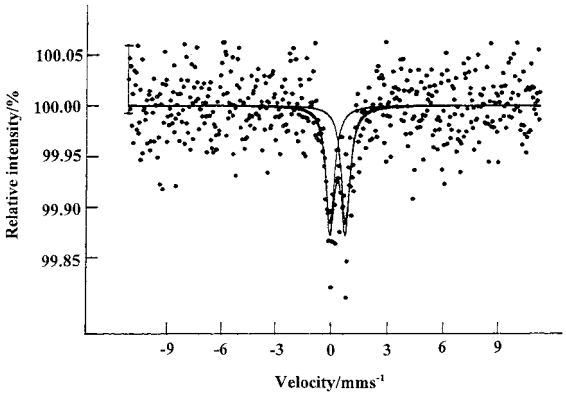

Figure 7. Mössbauer spectrum of TBA-**I** at 296 K. The solid line is a least-squares fit to the data.

the literature.[13] No bands due to $[\alpha\text{-}SiW_{11}\{Fe(OH_2)\}O_{39}]^{5-}$ (λ_{max} = 261 nm, $\epsilon = 4.75 \times 10^4$ M^{-1} cm^{-1}; λ_{max} = 473 nm, ϵ = 19 M^{-1} cm^{-1}) and $[\alpha\text{-}SiW_9\{Fe(OH_2)\}_3O_{37}]^{7-}$ (λ_{max} = 262 nm, $\epsilon = 3.80 \times 10^4$ M^{-1} cm^{-1}; λ_{max} = 461 nm, ϵ = 39 M^{-1} cm^{-1}) were observed, showing the high purity of TBA-**I**. The 470 nm band was not changed by the treatment with liquid Br_2, showing that the oxidation state of two iron centers is 3+.

Mössbauer Spectrum. The Mössbauer spectrum of TBA-**I** is shown in Figure 7.[39] The number and intensity of signals show the symmetry of two iron centers in TBA-**I**. The spectrum of TBA-**I** showed two equivalent signals, indicating that two iron centers are equivalent. A least-squares fit (solid line) to the experimental points gave the isomer shift, δ = 0.32 mm s^{-1}, and the quadrupole splitting, ΔE_Q = 0.81 mm s^{-1}. Values change with oxidation states of diiron atoms. The value of 0.32 mm s^{-1} is in the range of 0.3−0.6 mm s^{-1}, where the isomer shifts for high-spin Fe^{3+} complexes are typically observed.[40−42]

(37) Rocchiccioli-Deltcheff, C.; Fournier, M.; Franck, R.; Thouvenot, R. *Inorg. Chem.* **1983**, *22*, 207−216.

(38) The increase in the UV band numbers with the decrease in the symmetry of Keggin-type polyoxometalates, $T_d \rightarrow C_{3v} \rightarrow C_{2v}$ in the $\alpha \rightarrow \beta \rightarrow \gamma$ sequence, is probably explained as follows: The splitting of degenerate orbitals of W−O bonds with decreasing symmetry of Keggin-type polyoxometalates leads to an increase in number of W←O charge transfer bands.

(39) The observed Mössbauer spectrum was somewhat noisy in spite of high counts (over 1 million) per channel. Most of the counts were derived from the Compton components for the non-Mössbauer γ-rays emitted from the Co-57 source (e.g., 121 keV) since the Mössbauer γ-ray was substantially attenuated by coexisting tungsten atoms in TBA-**I**.

(40) Kessel, S. L.; Hendrickson, D. N. *Inorg. Chem.* **1978**, *17*, 2630−2636.

(41) Heistand, R. H., II; Roe, A. L.; Que, L., Jr. *Inorg. Chem.* **1982**, *21*, 676−681.

(42) Floriani, C.; Fachinetti, G.; Calderazzo, F. *J. Chem. Soc., Dalton Trans.* **1973**, 765−769.

Table 1. Comparison of Magnetic and Mössbauer Data for Diiron(III) Complexes, Oxidized MMO, and Oxidized RR[a]

		Mössbauer	
	J/cm^{-1}	δ/(mm s^{-1})	ΔE_Q/(mm s^{-1})
TBA-**I**	−5 to −1, antiferromagnetic	0.32 (296 K)	0.81 (296 K)
1	−95, antiferromagnetic	0.58 (300 K)	0.92 (300 K)
2	−2.5, antiferromagnetic	0.36 (295 K)	0.75 (295 K)
3	−119, antiferromagnetic	nr[b]	nr[b]
4	−6.9, antiferromagnetic	0.49	0.56
5	−11.7, antiferromagnetic	nr[b]	nr[b]
6	−132, antiferromagnetic	nr[b]	nr[b]
7	−119, antiferromagnetic	nr[b]	nr[b]
8	−17, antiferromagnetic	0.47	1.50
9	−134, antiferromagnetic	nr[b]	nr[b]
10	−15.4, antiferromagnetic	nr[b]	nr[b]
11	1.21, ferromagnetic	nr[b]	nr[b]
MMO_{ox}	−8, antiferromagnetic (d^5 high spin)	0.50	1.07
RR_{ox}	−108, antiferromagnetic (d^5 high spin)	0.53	1.65
		0.45	2.45

[a] **1**, $[Fe(salen)_2]O$ (salen = $C_{16}H_{14}N_2O_2^{2-}$);[44] **2**, $[Fe(salen)]_2Q$ (salen = $C_{16}H_{14}N_2O_2^{2-}$, Q = quinone moiety);[40] **3**, $[Fe_2O(C_{10}H_8N_2)_4(CH_3CO_2)(ClO_4)_3]$;[45] **4**, $[Fe_2(C_{16}H_{18}N_2O_2)_2(OH)_2]$;[46] **5**, $[(CH_3)_2NC_7H_2NO_4(H_2O)Fe(OH)]_2$;[47] **6**, $[Fe_2O(CH_3CO_2)Cl_2(bipy)_2]$ (bipy = 2,2′-bipyridine);[48] **7**, $[Fe_2O(CH_3CO_2)_2(Me_3TACN)_2](PF_6)_2$ (Me_3TACN = 1,4,7-trimethyl-1,4,7-triazacyclononane);[49] **8**, $[(HB(pz)_3)Fe(OH)(CH_3CO_2)_2Fe(HB(pz)_3)]^+$ ($HB(pz)_3$ = hydrotris(1-pyrazolyl borate ion);[50] **9**, $(C_5H_{12}N)_3[(CH_3CO_2)\{Fe(C_6H_4O_2)_2\}_2]$;[51] **10**, $[Fe_2L(OC_2H_5)_2Cl_2]$ (L = hexadentate Schiff base);[52] **11**, $[Fe_2(salmp)_2]$ (salmp = $C_{21}H_{18}N_2O_3$);[54] MMO_{ox}.[55,56] RR_{ox}.[55,56] [b] Not reported.

No signals due to ferrous irons were observed. ΔE_Q values reflect the environment surrounding the diiron core.[43] 0.81 mm s^{-1} is not in the range of 1.40−1.45 and 1.27−1.81 mm s^{-1} observed for five- or six-coordinate high-spin diferric μ-oxo dibridged and μ-oxo tribridged complexes, respectively.[43] The value is in the range of 0.53−0.97 mm s^{-1} observed for high-spin diferric μ-hydroxo dibridged complexes.[43] These results and NMR, infrared, Raman, and UV−visible data show that TBA-**I** has a γ-Keggin structure with C_{2v} symmetry and that the two diferric iron atoms occupy adjacent octahedra at 1 and 2 positions in Figure 1.

The δ and ΔE_Q values of TBA-**I**, diferric complexes,[40,44−54] oxidized methane monooxygenase (abbreviated as MMO_{ox}),[55,56] and oxidized ribonucleotide reductase (abbreviated as RR_{ox})[55,56] are summarized in Table 1. The δ and ΔE_Q values for TBA-**I** are close to those for MMO_{ox}, **1**, **2**, and **4** with the symmetrical iron centers, and different from those for RR_{ox} (δ_1 = 0.53 mm s^{-1}, ΔE_{Q1} = 1.65 mm s^{-1} and δ_2 = 0.45 mm s^{-1}, ΔE_{Q2} = 2.45 mm s^{-1}) with asymmetrical two iron centers and **8**.

Magnetic Susceptibility. Plots of molar susceptibility and effective moments vs temperature are shown in Figure 8. The

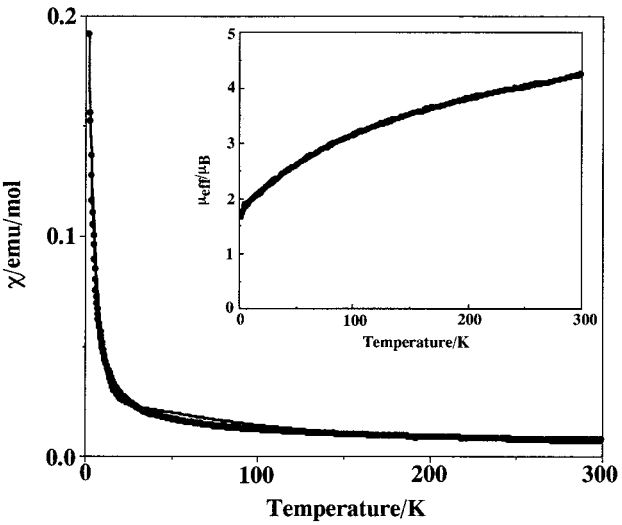

Figure 8. Magnetic susceptibility of TBA-**I** vs temperature. Solid line is a least-squares fit to the data with J = −0.88 cm^{-1}. Inset: The effective moment of TBA-**I** vs temperature.

theoretical magnetic moment (spin-only) is 11.0μ_B for a ferromagnetically coupled S = 5 system, and the magnetic moment for TBA-**I** was 4.2μ_B at 296 K, implying some extent of antiferromagnetic coupling.[57] Magnetic exchange in a binuclear species can be represented by the isotropic Heisenberg Hamiltonian, $H = -2JS_1 \cdot S_2$, where J is the magnitude of the intermolecular exchange interaction between spins S_1 and S_2. For TBA-**I**, S_1 and S_2 are $^5/_2$. The resulting magnetic susceptibility can be expressed by eq 2. The temperature-dependent

$$\chi = \frac{2Ng^2\mu_B{}^2}{kT}\frac{2e^{2x} + 10e^{6x} + 28e^{12x} + 60e^{20x} + 110e^{30x}}{1 + 3e^{2x} + 5e^{6x} + 7e^{12x} + 9e^{20x} + 11e^{30x}} \quad \left(x = \frac{J}{kT}\right) \quad (2)$$

magnetic behavior was analyzed with eq 2. The g value of 2.0

(43) Kurtz, D. M., Jr. *Chem. Rev.* **1990**, *90*, 585−606.
(44) Murray, K. S. *Coord. Chem. Rev.* **1974**, *12*, 1−35.
(45) Ménage, S.; Vincent, J. M.; Lambeaux, C.; Chottand, G.; Grand, A.; Fontecave, M. *Inorg. Chem.* **1993**, *32*, 4766−4773.
(46) Borer, L.; Thalken, L.; Ceccarelli, C.; Glick, M.; Zhang, J. H.; Reiff, W. M. *Inorg. Chem.* **1983**, *22*, 1719−1724.
(47) Ou, C. C.; Lalancette, R. A.; Potenza, J. A.; Schugar, H. J. *J. Am. Chem. Soc.* **1978**, *100*, 2053−2057.
(48) Vincent, J. B.; Huffman, J. C.; Christou, G. *J. Am. Chem. Soc.* **1988**, *110*, 6898−6900.
(49) Hartman, J. R.; Rardin, R. L.; Chaudhuri, P.; Pohl, K.; Weighardt, K.; Nuber, B.; Weiss, J.; Papaefthymiou, G. C.; Frankel, R. B.; Lippard, S. J. *J. Am. Chem. Soc.* **1987**, *109*, 7387−7396.
(50) Armstrong, W. H.; Lippard, S. J. *J. Am. Chem. Soc.* **1984**, *106*, 4632−4633.
(51) Anderson, B. F.; Webb, J.; Buckingham, D. A.; Robertson, G. B. *J. Inorg. Biochem.* **1982**, *16*, 21−32.
(52) Chiari, B.; Piovesana, O.; Tarantelli, T.; Zanazzi, P. F. *Inorg. Chem.* **1982**, *21*, 2444−2448.
(53) Chiari, B.; Piovesana, O.; Tarantelli, T.; Zanazzi, P. F. *Inorg. Chem.* **1982**, *21*, 1396−1402.
(54) Snyder, B. S.; Patterson, G. S.; Abrahamson, A. J.; Holm, R. H. *J. Am. Chem. Soc.* **1989**, *111*, 5214−5223.
(55) Valentine, A. M.; Lippard, S. J. *J. Chem. Soc., Dalton Trans.* **1997**, 3925−3931.
(56) Vincent, J. B.; O.-Lilley, G. L.; Averill, B. A. *Chem. Rev.* **1990**, *90*, 1447−1467.
(57) In Table 1, the magnetic moments of various diiron complexes were in the range of 1.9−8.3μ_B. The magnetic moment of 4.2μ_B for TBA-**I** was close to the 4.9μ_B of complex **5** with hydroxo/aqua bridging ligands.

was used for the analysis since the ESR spectrum of TBA-**I** at 4 K showed two broad signals at $g = 4.3$ and 2.0. The signal at $g = 4.3$ probably arises from the EPR active portion of adventitiously bound Fe^{3+}. Similar spectra and assignments have been reported.[53,58,59,] In the temperature range of 2−300 K, the calculated data fit well with observed data with $J = -0.88$ cm^{-1}, as shown in Figure 8. In the lower temperature range of 2−10.5 K, the best fit was obtained with $J = -3.7$ cm^{-1}. In both cases, J values did not much change. A J value of -5 to -1 cm^{-1} indicates the weak antiferromagnetic interaction between two ferric centers.

The J values of TBA-**I**, diferric complexes, **1**−**11**,[40,44−54] MMO_{ox},[55,56] and RR_{ox}[55,56] are also summarized in Table 1. The antiferromagnetic interaction ($J = -5$ to -1 cm^{-1}) for TBA-**I** is close to those of **2**, **4**, **5**, and hydroxo/aqua-bridged MMO_{ox}[43,44,47,55,56] and far from those of **3**, **6**, **7**, **8**, **9**, and oxo/acetato-bridged RR_{ox}[40,43,48−51,56] with one or two acetato bridges. Mössbauer and magnetic data for TBA-**I** are similar to those for **2**, **4**, and MMO_{ox}. Complex **4** and MMO_{ox} have hydroxo-bridged structures. The complex **2** has a quinone-bridged structure, different from that of TBA-**I**. Therefore, Mössbauer and magnetic data suggest that the core structure of TBA-**I** is hydroxo-bridged.

Conclusions

A diiron-substituted polyoxometalate, $[\gamma\text{-}SiW_{10}\{Fe(OH_2)\}_2O_{38}]^{6-}$, has been synthesized and isolated in 50% yield. The NMR, infrared, Raman and UV−visible spectra indicated that the complex has a γ-Keggin structure with C_{2v} symmetry and that two iron centers occupy adjacent, edge-shared octahedra. UV−visible, Mössbauer, ESR, and magnetic susceptibility data show that two high-spin Fe^{3+} centers are equivalent and antiferromagnetically coupled.

Acknowledgment. We acknowledge Profs. K. Kishio (The University of Tokyo) and J. Simoyama (The University of Tokyo), Prof. H. Nishihara (The University of Tokyo), and Dr. H. Yahiro (Hiroshima University) for the magnetic susceptibility, infrared (below 600 cm^{-1}), and ESR measurements, respectively. This work was supported in part by a Grant-in-Aid for Scientific Research from the Ministry of Education, Science, Sports and Culture of Japan.

IC9902065

(58) Fox, B. G.; Lipscomb, J. D. *Biochem. Biophys. Res. Commum.* **1988**, *154*, 165−170.
(59) Fox, B. G.; Froland, W. A.; Dege, J. E.; Lipscomb, J. D. *J. Biol. Chem.* **1989**, *264*, 10023−10033.
(60) Jeannin, Y.; Fournier, M. *Pure Appl. Chem.* **1987**, *59*, 1529−1548.